

DETECTING BRANCHING STRUCTURES USING LOCAL GAUSSIAN MODELS

Li Wang and Abhir Bhalerao

Department of Computer Science, University of Warwick, UK

{liwang, abhir}@dcs.warwick.ac.uk

ABSTRACT

We present a method for modelling and estimating branching structures, such as blood vessel bifurcations, from medical images. Branches are modelled as a superposition of Gaussian functions in a local region which describe the amplitude, position and orientations of intersecting linear features. The centroids of component features are separated by applying K-means to the local Fourier phase and the covariances and amplitudes subsequently estimated by a likelihood maximisation. We employ a penalised likelihood test (AIC) to select the best fit model in a region. Results are presented on synthetic and representative 2D retinal images which show the estimation to be robust and accurate in the presence of noise. We compare our results with a curvature scale-space operator method.

1. INTRODUCTION

The detection of line, corner and branching structures is a widely studied problem in computer vision, especially for object recognition, and is an important one for tasks such as image registration and segmentation in medical imaging. In this work, our aim is to derive a reliable method for the quantisation of branching structures from 2D and 3D medical imagery and apply it to problems such as segmenting the blood vessels from retinal images [1], and characterising the bronchial tree from 3D CT images [2].

Corner and branch point detection algorithms can be broadly classified into those that first estimate image boundaries or curves using image gradient operators of one sort or another and then infer the position of the junction, to those that directly apply a curvature measure or template to the grey level data. Methods that use the intersections of boundaries to label corners necessitate the thinning of curves to a single pixel width e.g. by skeletonisation. Because of ambiguities caused by the line thinning, the subsequent labelling of branch points can be problematic, particularly in 3D. In general, methods that use second or greater order differentials of the image intensity are sensitive to noise, whereas template approaches are limited in the range and type of

branch points that can be described [3]. Scale-space curvature provides some trade-off between these approaches because of the noise immunity gained by repeated smoothing, plus the ability to naturally model the size of features and, by tracking curvature through scale, allowing labelling decisions to be confirmed by comparing estimates at different scales in the feature space. The disadvantages are that branch points are not modelled explicitly and the implementation does not readily extend to 3D [4].

We propose a model based estimation that operates directly on the image intensities. Regions of the image are modelled locally as a superposition of M Gaussian functions and an iterative, ML estimation used to derive the parameters. Each Gaussian represents a single, approximately linear feature in the region which parameterised by a mean (centroid), an orientation and width (covariance), and an amplitude. Models for $M = 1, 2$ are fitted separately to the region and a penalised likelihood information measure, the Akaike Information Criteria (AIC), is used to choose the best for a given region size. The feature parameters are first separated using K-means by modelling the local phase-spectrum, which is linearly dependent on the component centroids. Having established an initial estimate of the component centroids, the feature covariances and amplitudes are estimated by a weighted maximisation that has similarities to EM.

After a description of the model and estimation algorithms, results are presented on a sample retinal fundus image. We conclude by discussion of the results and make proposals for further work.

2. FEATURE MODELLING AND SELECTION

2.1. Feature Modelling and Estimation

In the spatial domain, if a linear feature is windowed by a smooth function such as a cosine square, $\cos^2(\cdot)$, then it can be approximated by a n -dimensional Gaussian:

$$G(\vec{x}|\Theta) = A \exp(-(\vec{x} - \vec{\mu})^T C^{-1}(\vec{x} - \vec{\mu})/2) \quad (1)$$

where A is the amplitude, $\vec{\mu}$ is the mean vector and C is the covariance matrix. Multiple features within the same region (Figure 1(d)) are modelled as a superposition and the

spectrum is approximated as a sum of component spectra:

$$G(\vec{\omega}) = \sum_{m=1}^M |G_m(\vec{\omega})| \exp[-j\phi_m(\vec{\omega})] \quad (2)$$

In particular, the phase-spectrum of a component exhibits a phase variation which is dependent on the feature centroid. We assume that this phase variation is independent for each of the M components of the model [5]:

$$\phi(\vec{\omega}) = \sum_{m=1}^M \phi_m(\vec{\omega}_m) = -\frac{B}{2\pi} \sum_{m=1}^M \vec{\mu}_m \cdot \vec{\omega}_m \quad (3)$$

Feature components are estimated by first separating out the component centroids using K-means clustering. At each step of the clustering, the phase-spectrum of each component is reconstructed using the current estimate of its centroid starting with M random positions. Each spatial frequency coordinate of the data phase-spectrum is then assigned to the closest component value and the new centroid estimates calculated from these partitions. The process is repeated until the centroid positions stabilise (typically <10 iterations). The M spatial frequency coordinate partitions are subsequently used to estimate the orientations of the Gaussian components.

The covariance of each Gaussian component is inversely related to the moment of inertia tensor, T , of its magnitude spectrum:

$$T = \frac{1}{B^n} \sum \frac{\vec{\omega}\vec{\omega}^T |G(\vec{\omega})|}{\|\vec{\omega}\|} \quad (4)$$

By forming tensors T_m based on the coordinate partitions from the K-means, an estimate can be made of the component covariances, C_m . Performing PCA on T yields the principal axes of the features forming the branch point and the corresponding eigen values are the widths (as variances).

This Fourier based estimation is computationally efficient and accurate in noise free data but can be greatly improved against noise by maximising the inner product between the windowed data, $f_B()$, and the model, G :

$$\arg_{\Theta} \max \sum_{\vec{x}} f_B(\vec{x}) G_m(\vec{x}|\Theta) \quad (5)$$

The result is a set of iterative equations that calculate sample statistics weighted by $w^t(\vec{x}) = f_B(\vec{x}) G_m(\vec{x}|\Theta_t)$ that are similar to the expectation step of EM. Unlike EM however, the weights here are not probabilities and do not sum to 1. More importantly, the estimation implicitly takes into account the spatial arrangement of the data $f_B(\vec{x})$ relative to the intensity model $G(\vec{x})$ whereas EM estimates the underlying distribution from which $f_B(\vec{x})$ are drawn. For each feature m in the window, the parametric set Θ_{t+1} can be calculated by:

$$A_m^{t+1} = \sum_{\vec{x}} w^t(\vec{x}) / \sum_{\vec{x}} G_m^2(\vec{x}|\Theta_t) \quad (6)$$

$$\vec{\mu}_m^{t+1} = \sum_{\vec{x}} w^t(\vec{x}) \vec{x} / \sum_{\vec{x}} w^t(\vec{x}) \quad (7)$$

$$C_m^{t+1} = 2 \sum_{\vec{x}} w^t(\vec{x}) (\vec{x} - \vec{\mu}_t)(\vec{x} - \vec{\mu}_t)^T / \sum_{\vec{x}} w^t(\vec{x}) \quad (8)$$

where t denotes iteration number and Θ_0 is the estimate from the spectrum of $f_B()$ using Eqns: 3 and 4. Convergence is achieved rapidly in 3-5 iterations. Figure 1 shows estimates of two type of linear features in part of a 2D retinal angiographic image for single and multiple Gaussian models.

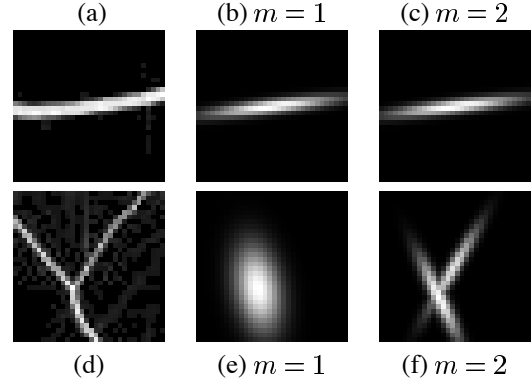


Fig. 1. (a)-(c): Estimation of a linear structure shown in (a) using single and multiple Gaussian intensity models (b),(c). (d)-(f): Estimation of branching structure shown in (d) using single and multiple models (e),(f). Block size is 32×32 .

2.2. Model Selection

Since we have multiple feature models, $m = 1, 2$, once the parameters of each model have been estimated, the accuracy of the hypothesis and the most fit model needs be determined in order to represent a given image region. We use a penalised distance measure, the Akaike information criterion (AIC), to bias the residual fit error which is expected to fall with increasing m . In minimum mean-square estimation, AIC is calculated using residual sums of squares (RSS)

$$AIC_m = B^n \ln(RSS/B^n) + 2P \quad (9)$$

where B^n is the number of data points in a square image region size B and P is the number of parameters in the model. The steps to finding the optimal model m_{opt} is summarised below:

1. Estimate the initial parameters for each model $m = 1..M$ for some block size B .
2. Use Eqns. 6-8 to improve the first estimate for each model m .
3. Compute AIC_m from RSS_m .
4. Repeat steps (1)-(3) for $m+1 \leq M$ (Eq. 9).
5. $m_{opt} = \arg_m \min(AIC_m)$.

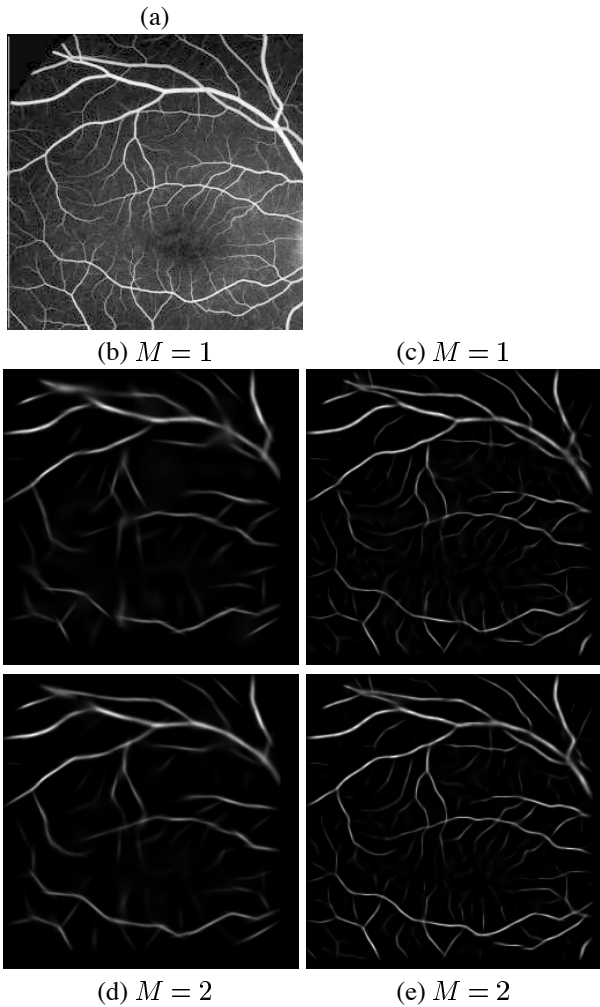


Fig. 2. (a) Part of human retinal angiographic image. (b)-(c) Single Gaussian model reconstructions at block sizes 32×32 and 16×16 . (d)-(e) Multiple Gaussian model reconstructions at 32×32 and 16×16 .

3. EXPERIMENTS AND DISCUSSION

In figure 2, the results of the ML model estimation and selection algorithm were tested by using a retinal image size 256×256 . The middle row shows reconstructions of the data using single feature model at two different scales using block sizes $B = 32, 16$. As expected, the model represents well vessel segments except those at or near branch points. The multiple feature model overcomes this (bottom row at figure 2). Overall, after the iterative ML estimation, the orientation, position and width of the features both along blood vessels and near bifurcations are accurately modelled. Based on the AIC selection scheme, we then attempted to select the best fit model, $m = 1, 2$, for each block and produced the data reconstruction shown in figure 3. Junction points are localised to regions where

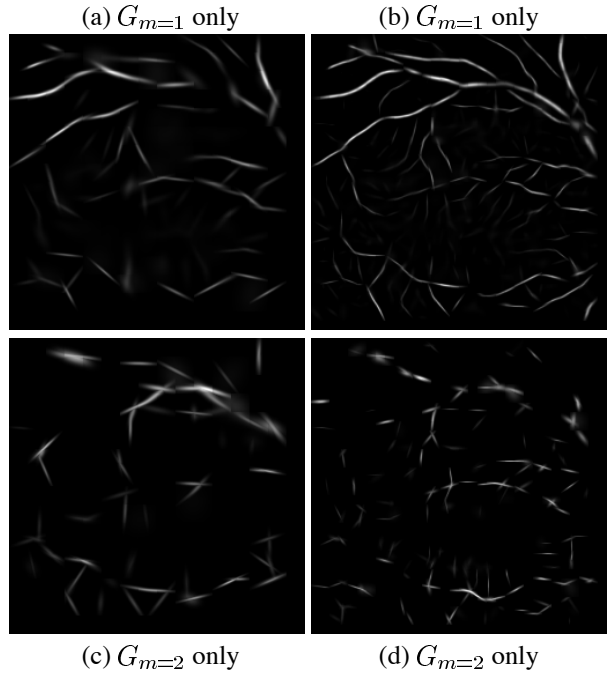


Fig. 3. (a)-(b) Reconstructions showing only single Gaussian model selections, $m = 1$. (c)-(d) Reconstructions showing only multiple Gaussian model selections, $m = 2$. (Block sizes $32 \times 32, 16 \times 16$)

$G_{m=2}$ is optimal. The feature intersection point can be trivially calculated from the model parameters, $\Theta_{m=1,2}$, in these blocks. In figure 4(a)-(b), the regions containing an inferred junction point or point of high curvature are highlighted by drawing a circle centred on the intersection and with the radius $B/2$ to indicate the detection scale.

As a means of comparison, we implemented a curvature scale-space method which has been widely used on edge or corner detections problem in computer vision.

Under this representation, for a 2D image $f(\vec{x})$, multi-scale spatial derivatives can be defined as

$$S_{\vec{x}^p}(\vec{x}|t) = f(\vec{x}) * \mathcal{G}_{\vec{x}^p}(\vec{x}|t) \quad (10)$$

where $\mathcal{G}_{\vec{x}^p}$ denotes a derivative of some order p of a Gaussian kernel [4].

After the whole stack of images is obtained, corner like features can be identified at different scales. In Lindeberg's work, the corner is detected by measuring the curvature of level curves, R , i.e. the change of gradient direction along an edge contour:

$$R = S_{x_2}^2 S_{x_1}^2 - 2S_{x_1} S_{x_2} S_{x_1 x_2} + S_{x_1}^2 S_{x_2}^2 \quad (11)$$

In one variation of this approach, as used here to produce Figure 4(c)-(d), the curvature is further multiplied by the gradient magnitude raised to the third power.

	No. of Junctions	False-positive	False-negative
Manual	65	0	0
Gaussian Model	60	80	5
Scale-space ($t = 0.1, 0.5, 1$)	32	118	33

Table 1. Results of validation with manual counting at one scale (16×16).

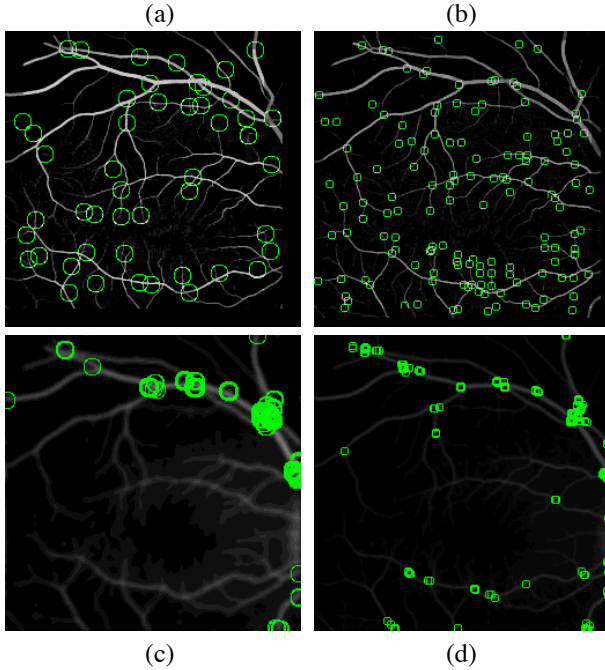


Fig. 4. (a)-(b) Branch point candidates labelled after model selection at block sizes 32×32 and 16×16 . (c)-(d) The 150 strongest corner responses of R from curvature scale-space representation at equivalent scales. (The radii of the circles reflect the detection scales).

Comparing the results given in figure 4 we observe that using the Gaussian model a greater number of the junction points or corners are detected than by the scale-space curvature. The scale-space method fails to find many of the branches at small scales, although this could be perhaps improved by parameter tuning. We attempted to validate our detector by noting the numbers of false-positive and false-negative labellings compared with a visual inspection and the curvature scale-space method, table 1. Our estimator produces some failures (mostly false-positives) in the retinal image but compares well with the scale-space results. Also like the curvature scale-space, it does not distinguish between true junctions and points of high curvature (corners). In terms of computational efficiency, our estimator is approximately equivalent to a pair of 9×9 spatial convolution operators, which is an order or magnitude better than a

curvature scale-space implementation.

4. CONCLUSIONS

We have described a modelling and estimation method that uses a superposition of Gaussian functions to model the local image intensity. The methods can be usefully applied to the detection and quantification of tree-like structures in medical images. The estimator is cheap to compute and robust in the presence of uncertainties in the image due to low signal to noise ratios and our preliminary results seem to compare favourably with curvature scale-space approaches, although objective validation is necessary. The next steps of this work will consider combining results of the estimator from different region sizes or scales to confirm the junction point detection and determine a ‘natural’ scale for the features which fit the single or multiple feature model for a given region size. Work toward a complete segmentation of the image will need a neighbourhood linking strategy to track features from region to region, perhaps within a Bayesian framework [6]. We are implementing our estimator in 3D to use on bronchus CT data.

5. REFERENCES

- [1] M. E. Martinez-Perez, A. D. Hughes, A. V. Stanton, S. A. Thom, A. A. Bharath, and K. H. Parka, “Retinal blood vessel segmentation by means of scale-space analysis and region growing,” in *Proceedings of the International Conference on Image Processing*, 1999, vol. 2, pp. 173–176.
- [2] V. Sauret, K. A. Goatman, J. S. Fleming, and A. G. Bailey, “Semi-automated tabulation of the 3d topology and morphology of branching networks using CT: Application to the airway tree,” in *Phys. Med. Biol.*, 1999, p. 44.
- [3] R. Mehrotr, S. Nichani, and N. Ranganathan, “Corner detection,” *Pattern Recognition*, vol. 23(11), pp. 1223–1233, 1990.
- [4] T. Lindeberg, “Junction detection with automatic selection of detection scales and localization scales,” in *Proc. 1st International Conference on Image Processing*, Nov. 1994, vol. 1, pp. 924–928.
- [5] A. R. Davies and R. Wilson, “Curve and corner extraction using the multiresolution fourier transform,” in *Image Processing and its Applications*. 4th IEE Conf., 1992.
- [6] A. Bhalerao, E. Thönnies, W. Kendall, and R. Wilson, “Inferring vascular structure from 2d and 3d imagery,” in *Medical Image Computing and Computer-Assisted Intervention*, 2001.